# On the suitability of two-layer energy-balance models for representing deep ocean heat uptake

Peter Shatwell, Arnaud Czaja, David Ferreira

May 2020

Coupled atmosphere-ocean general circulation models (AOGCMs) have grown greatly in complexity, commensurate with advances in computing technologies over the last few decades. They are tremendously useful and comprehensive tools to study the climate and perform projections, yet they are computationally very expensive. An alternative is to use simple climate models to emulate the AOGCM responses, covering a wider range of potential climate scenarios with negligible computational cost. One branch of simple climate models encompasses physically-based energy balance models (EBMs). They can be useful in summarising and comparing the properties of different AOGCMs [Gregory and Forster, 2008, Raper et al., 2002], and their parameters can be interpreted in terms of real physical processes (e.g. [Kostov et al., 2014]) so may provide insight into the underlying physics.

Here, we examine the two-layer energy balance model as presented in [Geoffroy et al., 2013] and fit it to step-function $CO_2$-doubling temperature responses of a coupled atmosphere-ocean-cryosphere general circulation model (GCM) with an idealised geometry with small and large basins. We assess the EBM-fitted responses, and find that the fits for the deep ocean response are poor. We propose a different two-layer EBM formulation motivated by the wind-driven circulation theory of [Rhines and Young, 1982b], and this improves fits for all the basins, but most significantly for the large basin (most representative of the global ocean).

## 1 GCM description

The model uses the Massachusetts Institute of Technology general circulation model (MITgcm) code [Marshall et al., 1997a, Marshall et al., 1997b]. Both the atmosphere and ocean component models use the same cubed-sphere grid at a C24 resolution (24x24 points per face, giving a resolution of 3.75° at the equator). The atmosphere has a low vertical resolution of five levels, and its physics is based on the 'simplified parameterisations primitive-equation dynamics' (SPEEDY) scheme [Molteni, 2003]. The ocean is flat-bottomed with a constant depth of 3 km, and is split into 15 levels with increasing vertical resolution from 30 m at the surface to 400 m at depth.

Mesoscale eddies are parameterised as an advective process [Gent and Mcwilliams, 1990] and an isopycnal diffusion [Redi, 1982], both with a transfer coefficient of 1200 $m^2\ s^{-1}$.

Ocean convection is represented by an enhanced vertical mixing of temperature and salinity [Klinger et al., 1996], while the background vertical diffusion is uniform and set to 3 $\times$ $10^{-5}$ $m^2$ $s^{-1}$. There are no sea-ice dynamics, but a simple two and a half layer thermodynamic sea-ice model [Winton, 2000] is incorporated. The seasonal cycle is represented, but there is no diurnal cycle.

The model is configured with the idealised 'Double-Drake' (DDrake) geometry (shown in figure 1) as seen in previous work (e.g. [Ferreira et al., 2010, Ferreira et al., 2015, Ferreira and Marshall, 2015]), which is an aquaplanet with two narrow vertical barriers that extend from the sea floor to the sea surface. The barriers are set 90° apart at the North Pole and extend meridionally to 35°S. This separates the ocean into small and large basins, with both of them connected by a 'southern ocean' region south of 35°S. The small and large basins in this configuration exhibit distinctive Atlantic-like and Pacific-like characteristics, with the small basin being warmer and saltier, and exhibiting a deep interhemispheric MOC (figure 2). The model geometry captures two important asymmetries relevant to the Earth's climate: a zonal asymmetry splitting the ocean into small and large basins, and a meridional asymmetry allowing for circumpolar flow in the Southern Hemisphere, but not in the Northern Hemisphere.

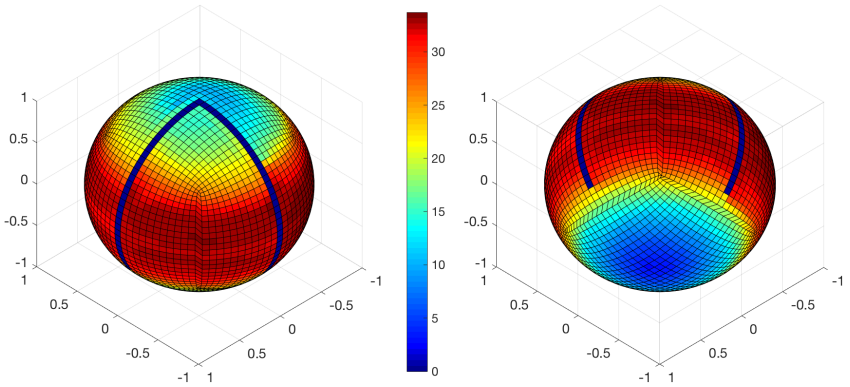


Figure 1: Time-averaged sea surface temperature (in °C) in the control integration, showing the model DDrake geometry.

The model is spun up for 6000 years until a statistically steady state is reached. The time-mean of the last 50-year integration is used as the equilibrated control climate state. We abruptly change the longwave absorption in the $CO_2$ band, causing an initial top-of-atmosphere forcing of approximately 4.4 W $m^{-2}$, thus mimicking an abrupt doubling of atmospheric $CO_2$ [Myhre et al., 1998], and run for an additional 200 years. The imposed EEI results in a warming of the climate system, and we diagnose the ensuing global and basin responses relative to the control climate.

# 2 Theoretical framework

The two-layer energy balance model (EBM) is a simple representation of the climate system, and can be used to help understand equilibrium and transient climate responses to different forcings. The climate system is split into two layers; the first layer, for our purposes, represents the oceanic mixed layer, and the second layer represents the deeper

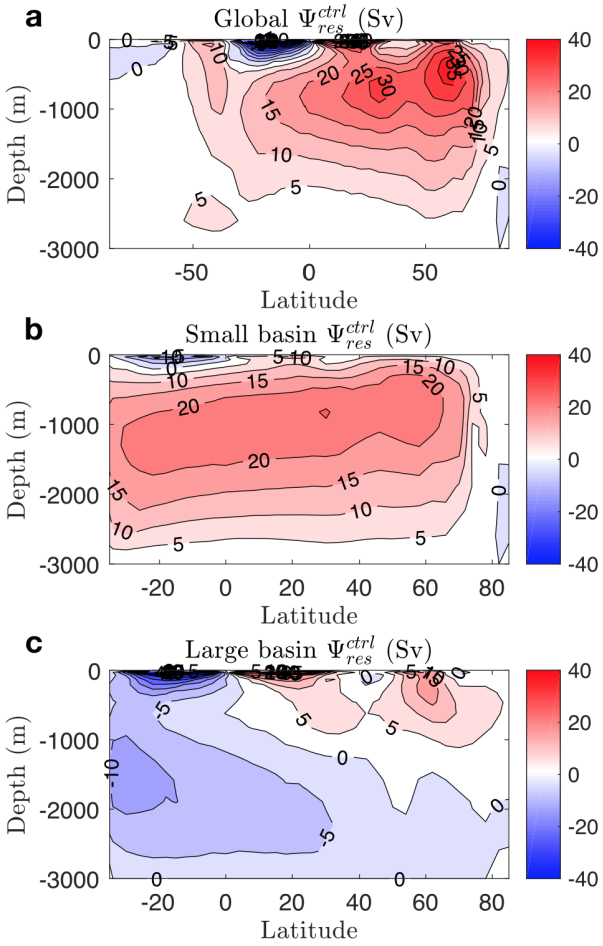


Figure 2: Control residual overturning streamfunctions for the (a) global, (b) small basin, and (c) large basin regions of DDrake (in Sv).

ocean below. The state of each layer is described by the temperature perturbations $T$ and $T_0$, and these change according to energy fluxes at the top of the atmosphere and an energy flux between the two layers. Following the notation in [Geoffroy et al., 2013] (except with $\lambda \leftrightarrow \alpha$), the temperature perturbations obey the equations:

$$\begin{aligned} C\frac{dT}{dt} &= \mathcal{F} - \alpha T - \gamma(T - T_0) \\ C_0\frac{dT_0}{dt} &= \gamma(T - T_0) \end{aligned} \tag{1}$$

Here, $\mathcal{F}$ is a top-of-atmosphere radiative forcing (W m$^{-2}$); for a step-function $CO_2$-doubling, $\mathcal{F}$ is a constant. The parameter $\alpha$ encompasses different radiative feedbacks of the system, and $\gamma$ parameterises the heat-exchange between the two layers. The constants $C$ and $C_0$ are effective heat capacities for each layer (J m$^{-2}$ K$^{-1}$). A diagram of the energy fluxes in the model is shown in figure 3.

We can rewrite equations 1 as a matrix differential equation in the form $d\mathbf{X}/dt =$

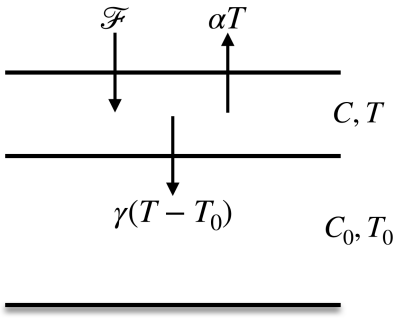


Figure 3: Diagram of the simple two-layer energy balance model. Arrows represent energy fluxes. $\mathcal{F}$ is the radiative forcing, $\alpha$ is the radiative feedback parameter, $\gamma$ is the heat exchange parameter, $T$ and $T_0$ are temperature perturbations, and $C$ and $C_0$ are effective heat capacities.

$\mathbb{A}\mathbf{X} + \mathbf{B}$:

$$\frac{d}{dt}\begin{pmatrix} T \\ T_0 \end{pmatrix} = \begin{pmatrix} -(\alpha+\gamma)/C & \gamma/C \\ \gamma/C_0 & -\gamma/C_0 \end{pmatrix}\begin{pmatrix} T \\ T_0 \end{pmatrix} + \begin{pmatrix} \mathcal{F}/C \\ 0 \end{pmatrix} \tag{2}$$

This can be solved to give:

$$\boxed{\begin{aligned} T(t) &= T_{eq}(1 - a_f e^{-t/\tau_f} - a_s e^{-t/\tau_s}) \\ T_0(t) &= T_{eq}(1 - \phi_f a_f e^{-t/\tau_f} - \phi_s a_s e^{-t/\tau_s}) \end{aligned}} \tag{3}$$

where $T_{eq} = \mathcal{F}/\alpha$ is the temperature at equilibrium, and the parameters $a_f, a_s, \tau_f, \tau_s, \phi_f$, and $\phi_s$ are as defined in [Geoffroy et al., 2013]. As $t \to \infty$, both $T$ and $T_0$ tend towards the equilibrium temperature $T_{eq}$. The parameters $\tau_f$ and $\tau_s$ are distinct fast and slow timescales, respectively. The fast timescale corresponds to the timescale of adjustment of the upper layer to the equilibrium temperature, while the slow timescale corresponds to a joint adjustment of the upper and lower layers. The parameters $a_f, a_s, \phi_f$, and $\phi_s$ are 'mode parameters' that partition the adjustment towards equilibrium into the fast and slow components such that $a_f + a_s = 1$ and $\phi_f a_f + \phi_s a_s = 1$.

# 3 Fitting procedure

We follow the same procedure as in [Geoffroy et al., 2013], where they successfully fit this two-layer EBM to CMIP5 model surface air temperature (SAT) responses to an abrupt $CO_2$-quadrupling, however, we fit to annually averaged SAT anomalies relative to the DDrake control climate rather than monthly snapshots. The radiative parameters $\mathcal{F}$ and $\alpha$ are found by linearly regressing the first 50 years of the net radiative imbalance against the global mean surface air temperature response, following the method of [Gregory et al., 2004]. The mode parameters are found making use of the analytical solutions in equations 3. For $t \gg \tau_f$, $T \approx T_{eq}(1 - a_s e^{-t/\tau_s})$, hence:

$$\ln\left(1 - \frac{T}{T_{eq}}\right) \approx \ln a_s - \frac{t}{\tau_s} \tag{4}$$

Then, the linear regression of $\ln(1 - T/T_{eq})$ against $t$ over the full 200 years provides estimates of $a_s$ and $\tau_s$, and then $a_f = 1 - a_s$. From the equation for $T$ in 3, we can re-arrange for $\tau_f$ giving:

$$\tau_f = \frac{t}{\ln a_f - \ln(1 - T/T_{eq} - a_s e^{-t/\tau_s})} \tag{5}$$

The value for $\tau_f$ is estimated by averaging over the first 10 years of the step-forcing experiment. Finally, $C, C_0$, and $\gamma$ (and $\phi_f$ and $\phi_s$) can be found through analytical relationships between these fitted parameters. Note that $C$ and $C_0$, and hence the layer thicknesses, are determined *a posteriori*.

Throughout this fitting procedure, only the global mean *surface air temperature* response is used. The EBM radiative and mode parameters are fitted to each CMIP5 model output in order to reproduce the SAT response. Arguably, this is a practical choice as humans live in the atmospheric surface boundary layer, so the SAT is most relevant to us when making climate projections. However, if we wish to be consistent with the *meaning* of the symbols in the two-layer EBM, $T$ is not the SAT response; it is the upper layer temperature response, which in this case is the oceanic mixed-layer temperature. The logic is thus flawed here, as the authors in [Geoffroy et al., 2013] conflate the EBM's predicted mixed-layer temperature with a surface air temperature, and these are quite different things (if they were the same, there would be no atmosphere-ocean sensible heat fluxes). Moreover, the EBM-predicted $T_0$ and its correspondence with a deep temperature response in the CMIP5 models is not examined.

# 4 Results and Discussion – DDrake fitted responses

Here, we present results for the two-layer 'Geoffroy EBM' fits to the DDrake temperature responses to an abrupt $CO_2$-doubling. The fitting procedure is performed for the globally-averaged response, and also for the basin-average responses for the small and large basins, and the model southern ocean. The effective layer heat capacities $C$ and $C_0$ (in W yr $m^{-2}$ $K^{-1}$) are found using the relationships:

$$\begin{aligned} C &= \frac{\alpha}{a_f/\tau_f + a_s/\tau_s} \\ C_0 &= \alpha(\tau_f a_f + \tau_s a_s) - C \end{aligned} \tag{6}$$

and the corresponding upper and lower layer thicknesses ($h$ and $H$, respectively) can thus be found using:

$$\begin{aligned} h &= \frac{86400 \times 360 \times C}{\rho_0 c_p} \\ H &= \frac{86400 \times 360 \times C_0}{\rho_0 c_p} \end{aligned} \tag{7}$$

where $\rho_0$ is a reference seawater density, and $c_p$ the specific heat capacity of seawater. In this way, the fitted EBM parameters give 'predictions' for the mixed-layer depth ($h$) and the depth to which the deep-ocean is thermally involved over the 200 years ($h + H$). If we subsequently plot the vertically-averaged DDrake temperature responses that correspond to these predicted layer thicknesses, we can assess how well the EBM actually captures

the process of deep ocean heat uptake i.e. the transfer of heat from the mixed-layer to the thermocline and deeper waters below. This transfer is characterised by the heat transfer coefficient $\gamma$ (W m$^{-2}$ K$^{-1}$) and is calculated with the relationship:

$$\gamma = \frac{C_0}{\tau_f a_s + \tau_s a_f} \tag{8}$$

These physical parameters (along with the fitted slow and fast timescales) are displayed in table 1. Radiative parameters and corresponding equilibrium temperatures are shown in table 2.

| | $C$ (W yr m$^{-2}$ K$^{-1}$) | $C_0$ (W yr m$^{-2}$ K$^{-1}$) | $h$ (m) | $H$ (m) | $\gamma$ (W m$-2$ K$^{-1}$) | $\tau_s$ (yr) | $\tau_f$ (yr) |
|---|---|---|---|---|---|---|---|
| Global | 20.3 | 108.1 | 153 | 817 | 1.02 | 185 | 7.9 |
| SB | 21.5 | 113.6 | 163 | 859 | 1.48 | 141 | 6.1 |
| LB | 21.3 | 109.0 | 161 | 824 | 1.39 | 141 | 6.3 |
| SO | 14.7 | 98.8 | 111 | 747 | 0.55 | 313 | 10.7 |

Table 1: Mixed-layer heat capacity $C$, deep-ocean heat capacity $C_0$, the corresponding mixed-layer and deep-ocean layer thicknesses $h$ and $H$, heat exchange coefficient $\gamma$ , and fitted slow and fast timescales $\tau_s$ and $\tau_f$ for each of the DDrake basins.

| | $\mathcal{F}$ (W m$^{-2}$) | $\alpha$ (W m$-2$ K$^{-1}$) | $T_{eq}$ (K) |
|---|---|---|---|
| Global | 4.44 | 1.48 | 3.00 |
| SB | 4.64 | 1.92 | 2.42 |
| LB | 4.73 | 1.90 | 2.49 |
| SO | 3.93 | 0.79 | 4.97 |

Table 2: Calculated radiative parameters for each of the DDrake basins: the radiative forcing $\mathcal{F}$, the radiative feedback $\alpha$, and the corresponding equilibrium temperature $T_{eq}$.

The mixed-layer heat capacities are approximately five times smaller than that of the deep ocean. The corresponding mixed-layer depths (MLDs) are thus fairly large (MLDs are typically ∼50-100 m [de Boyer Montégut et al., 2004]). However, it is difficult to determine the meaning of these values as the DDrake configuration used does not represent an oceanic mixed-layer, not presently incorporating the KPP vertical mixing scheme [Large et al., 1994].

The global value for $h + H$ gives a total ocean depth of 970 m, close to the CMIP5 ensemble mean found in [Geoffroy et al., 2013] of 1105 m. The $H$ values seem too low, however, as the overturning cells in figure 2 extend far below 1 km depth, especially in the small basin. Nevertheless, the small basin's effective heat capacity (and corresponding depth) is the largest, as well as its heat exchange $\gamma$. This is expected as it has a deep overturning circulation, yet the difference between the small and large basin parameters here is modest. Perhaps surprisingly, the DDrake southern ocean has the smallest effective heat capacity, with an associated small value of $\gamma$, in contrast with the

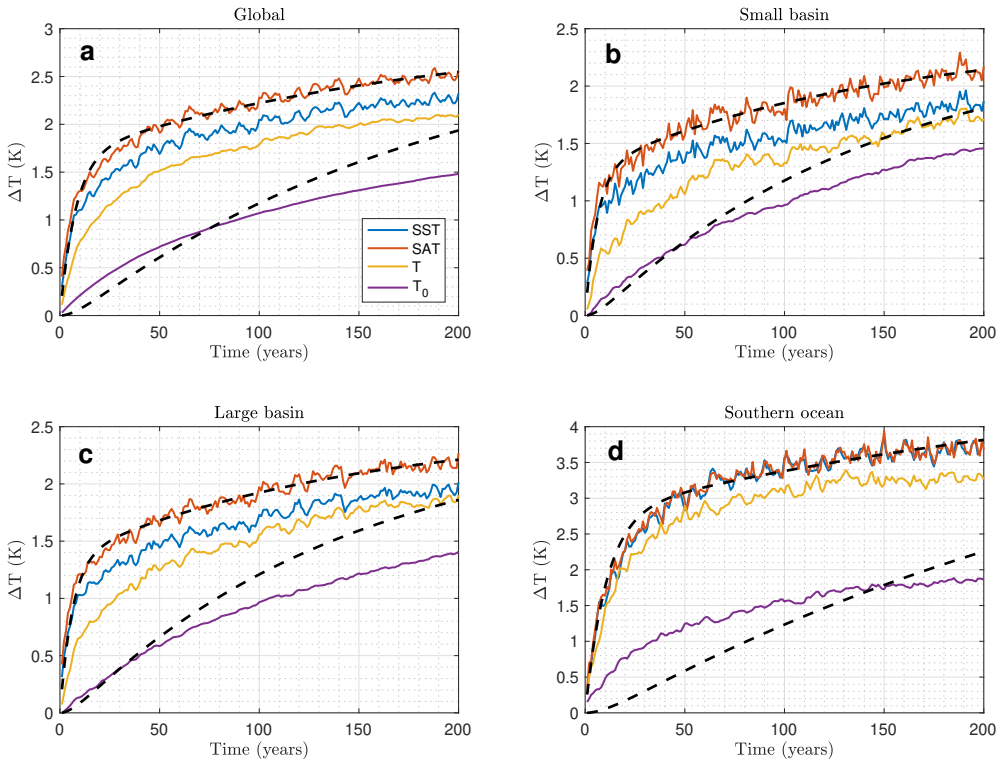


Figure 4: Time-series of annually-averaged surface air temperature (SAT, orange line) and sea surface temperature (SST, blue line); and vertically-averaged upper layer temperature ($T$, yellow line) and lower layer temperature ($T_0$, purple line) corresponding to the derived layer thicknesses presented in table 1 for the (a) global, (b) small basin, (c) large basin, and (d) southern ocean regions of DDrake, relative to the control climate state. The fitted Geoffroy EBM responses for $T$ and $T_0$ are shown as black dashed lines.

Southern Ocean's (capitalised) dominance in global ocean heat uptake in CMIP5 models [Frölicher et al., 2015].

The fitted EBM responses are shown in figure 4. The EBM (black dashed lines) reproduces the DDrake surface air temperature response not only globally, but also regionally for each basin. This is unsurprising as the SAT response is what the EBM radiative and mode parameters were fitted to, and this is what was found and presented for CMIP5 models in [Geoffroy et al., 2013]. However, if we compare the EBM fits to the sea surface temperature (SST) responses, a good fit is only seen for the southern ocean (figure 4, panel d), where the SST and SAT are comparable. Globally, and in the small and large basins, the SAT is $\approx 0.2$ K warmer than the SST.

Even worse, the temperature responses corresponding to the EBM-predicted upper-layer thicknesses $h$ as presented in table 1 (yellow lines) show very little correspondence with the upper-layer black dashed fits. The same is true for the lower-layer responses (purple lines). As mentioned in section 3, if we wish to be consistent with the original formulation of the two-layer EBM, the fitted black dashed lines for $T$ and $T_0$ should correspond to the yellow and purple lines respectively in figure 4. Evidently, they do not.

So, although the SAT response is well-reproduced, the other curves suggest this two-layer EBM is a poor representation of ocean heat uptake.

Root mean-square errors for each of these fits evaluated against the yellow and purple lines are shown in table 3. The small basin and southern ocean span the extremes; the small basin has the poorest upper-layer fit, but the best lower-layer fit, while the southern ocean is the opposite. Taking both layers together, the EBM captures the small and large basin responses almost equally well, with the worst overall fit found for the southern ocean.

| | Upper layer $T$ RMSE (K) | Lower layer $T_0$ RMSE (K) | Total RMSE (K) |
|---|---|---|---|
| Global | 0.45 | 0.23 | 0.68 |
| SB | 0.47 | 0.21 | 0.68 |
| LB | 0.39 | 0.28 | 0.67 |
| SO | 0.37 | 0.40 | 0.77 |

Table 3: Root mean-square errors for the EBM fits for the upper and lower layer temperature responses $T$ and $T_0$ for each basin of DDrake.

# 5 A new EBM framework

## 5.1 Vertical structure of the wind-driven circulation

This is a very brief treatment of the main results from [Rhines and Young, 1982b], leading to an expression for the theoretical vertical heat transport, $w\theta$, within a wind-driven gyre. All of what follows is grounded in quasigeostrophic theory. It's found that $w\theta \propto (\partial\theta/\partial z)^2$, meaning that any layered energy-balance model that represents heat exchanges between layers via temperature differences or a vertical temperature gradient may be inaccurate when attempting to describe heat uptake dominated by wind-driven gyres.

### 5.1.1 Streamfunction solution

Ignoring relative vorticity (appropriate for basin-scale circulations), the quasigeostrophic potential vorticity (PV) in a wind-driven gyre is given by:

$$q = \beta y + \frac{f_0^2}{N^2}\frac{\partial^2\psi}{\partial z^2} \tag{9}$$

where $f_0$ is a reference value for the Coriolis parameter, $\beta$ is its variation with latitude, and $N$ is the buoyancy frequency. Removing the dimensions, this becomes:

$$\hat{q} = \hat{y} + \frac{\partial^2\hat{\psi}}{\partial\hat{z}^2} \tag{10}$$

We define a depth $D(x, y)$ that marks the lower boundary of the wind-driven gyre (bowl); below this depth, $\psi = 0$. If we assume $\hat{q} = y_0 = const.$ is the non-dimensional PV value

within the gyre (from PV homogenisation arguments [Rhines and Young, 1982a]), and we drop the hats, the equations we need to solve are:

$$\psi_{zz} + y = y_0 \qquad ; \qquad -D(x,y) < z < 0 \tag{11}$$

$$\psi = 0 \qquad ; \qquad z \leq -D(x,y) \tag{12}$$

At the lower boundary of the bowl, we require $\psi = \psi_z = 0$ to ensure that $\psi$ and $\psi_z$ remain continuous across the boundary. This leads to the solution:

$$\psi = \frac{1}{2}(z+D)^2(y_0 - y) \qquad ; \qquad -D(x,y) < z < 0 \tag{13}$$

We can obtain an expression for $D$ using the non-dimensional buoyancy equation and rearranging for $w$, giving:

$$w = -J(\psi, \psi_z) = -\frac{\partial \psi}{\partial x}\frac{\partial \psi_z}{\partial y} + \frac{\partial \psi}{\partial y}\frac{\partial \psi_z}{\partial x} \tag{14}$$

N.B. we are only interested in statistically-steady solutions. At the surface, $\psi|_{z=0} = \frac{D^2}{2}(y_0 - y)$ and $\psi_z|_{z=0} = D(y_0 - y)$, which means that the Ekman pumping velocity, $w_E \approx w|_{z=0}$, is:

$$w_E \approx w|_{z=0} = \frac{D^2}{2}\frac{\partial D}{\partial x}(y_0 - y) \tag{15}$$

We define the non-dimensional barotropic streamfunction as:

$$\psi_B = \int_x^{x_E} w_E dx' \tag{16}$$

where $x_E$ is the eastern boundary of the gyre. So, integrating the expression for $w_E$ and rearranging for $D$ gives us:

$$D = \Big(\frac{6\psi_B}{y_0 - y}\Big)^{1/3} \tag{17}$$

This can be substituted back into our expression for $\psi$ giving the full streamfunction solution.

### 5.1.2 Vertical heat-transport

We've already seen that the (non-dimensional) expression for the vertical velocity is $w = -J(\psi, \psi_z)$. The non-dimensional expression for the temperature is simply $\theta = \psi_z$. Hence, the vertical heat-transport has the form:

$$w\theta = \psi_z(\psi_y \psi_{zx} - \psi_x \psi_{zy}) \tag{18}$$

Expanding this out gives you:

$$\begin{aligned} w\theta = (z+D)(y_0 - y)\Big[\big[(z+D)D_y(y_0 - y) - \frac{1}{2}(z+D)^2\big]D_x(y_0 - y) \\ - (z+D)D_x(y_0 - y)\big[D_y(y_0 - y) - (z+D)\big]\Big] \end{aligned} \tag{19}$$

And, after cancelling and simplifying, we're left with only one term for the equation, giving the expression for the vertical heat-transport:

$$w\theta = \frac{1}{2} D_x (z + D)^3 (y_0 - y)^2 \tag{20}$$

This is the analytical form for the vertical heat-transport within the bowl, and depends only on $\psi_B$, which is ultimately determined by the surface wind-stress. Note that $\partial\theta/\partial z = \psi_{zz} = y_0 - y$, hence we can also write equation 20 as:

$$w\theta = \frac{1}{2} D_x (z + D)^3 \theta_z^2 \tag{21}$$

In the two-layer EBM described in section 2, the heat flux from the upper layer to the lower layer depends on the temperature difference between the two layers: $H_\downarrow = \gamma(T - T_0)$. This is the simplest representation of a temperature gradient with depth, i.e. $\theta_z$. The presence of $\theta_z^2$, rather than $\theta_z$, in the expression for the vertical heat transport in equation 21 suggests that the linear heat exchange $\gamma(T - T_0)$ is unsuitable in modelling heat uptake in a wind-driven gyre. A more accurate representation may be $H_\downarrow = \gamma^*(T - T_0)^2$. Our new 'Rhines/Young' (RY) EBM equations to try are thus:

$$\begin{aligned} C\frac{dT}{dt} &= \mathcal{F} - \alpha T - \gamma^*(T - T_0)^2 \\ C_0\frac{dT_0}{dt} &= \gamma^*(T - T_0)^2 \end{aligned} \tag{22}$$

## 5.2 Results and Discussion – New DDrake fitted responses

In section 3, the fitting of the mode parameters for the Geoffroy EBM relies on prior knowledge of the analytical solution to the equations 1, but we do not know what the analytical solution is for the RY EBM equations 22. Also, in order to compare the two different EBM formulations, we should use the same fitting procedure for both; hence we cannot follow the same procedure as in section 3. Instead, we take a more empirical approach.

The radiative parameters $\mathcal{F}$ and $\alpha$ are still found in the same way using the [Gregory et al., 2004] method, but fitting to the global SST rather than the SAT response. To find the mode parameters, we prescribe the layer thicknesses $h = 50$ m and $H = 1000$ m (setting $C$ and $C_0$), and vary the heat exchange parameters $\gamma$ and $\gamma^*$ for the Geoffroy and RY EBMs, respectively, so as to minimise the RMSE of the fits. The optimal values for $\gamma$ and $\gamma^*$ found in this way for each of the DDrake basins are shown in table 4. Again, the largest values are found for the small basin where there is a deep overturning circulation.

The new fitted EBM responses found using this method are shown in figure 5. The upper layer temperature responses are captured fairly well by both of the EBMs, apart from in the southern ocean where the fit is poor. The lower layer temperature responses in the small and large basins are captured particularly well, with the RY EBM performing better than the Geoffroy EBM. It is more instructive to see the percentage improvement in the RMSE of the fits upon moving from the Geoffroy EBM to the RY EBM, and this is shown in figure 6.

| | $\gamma$ (W m$^{-2}$ K$^{-1}$) | $\gamma^*$ (W m$^{-2}$ K$^{-2}$) |
|---|---|---|
| Global | 1.20 | 1.12 |
| SB | 1.56 | 1.91 |
| LB | 1.24 | 1.28 |
| SO | 0.73 | 0.38 |

Table 4: Optimised heat exchange parameter values for the Geoffroy and RY EBMs, which minimise the RMSE of the fitted DDrake temperature responses.

Notably, the switch to the RY EBM improves the overall fits for *all* the DDrake basins (blue bars), albeit only by ∼10%. We see more striking increases for the lower layer responses, especially for the large basin, with a lower layer fit improvement of +55%. A similar improvement of +47% is found for the lower layer small basin response, yet this is at the (small) expense of the upper layer. The RY EBM equations 22 were inspired by wind-driven circulation theory [Rhines and Young, 1982b], so it is reassuring that the largest fit improvements are seen for the large basin where wind-driven circulations dominate (figure 2). Like the real-world Pacific ocean, the large basin also dominates the global average SST response. These results suggest that the RY EBM (equations 22) is better able to capture both the surface and deep ocean temperature responses than the Geoffroy EBM (equations 1). It may also be more physically relevant, especially if global ocean heat uptake is dominated by wind-driven gyres.

# 6 Conclusion

Using the two-layer EBM framework of [Geoffroy et al., 2013], we successfully fitted surface air temperature (SAT) responses for each of the DDrake basins under an abrupt $CO_2$-doubling experiment. However, as noted in section 3, the meaning of $T$ in the EBM is the temperature response of the upper-layer (here, the oceanic mixed layer), not the SAT response. Calculating the EBM-predicted layer temperature responses using equations 1, and comparing with the DDrake temperature responses corresponding to the EBM-predicted layer thicknesses (table 1), we find that the fits are poor (figure 4). This suggests that although the SAT is well-reproduced, this EBM is a poor representation of ocean heat uptake in DDrake.

We proposed a new EBM framework (equations 22) motivated by wind-driven circulation theory [Rhines and Young, 1982b] which parameterises the ocean ventilation rate as a quadratic heat exchange (rather than linear) between the two layers. By changing to this framework, we find that all the fitted DDrake temperature responses are improved upon, with a total global improvement of +17% (figure 6). The largest improvement is found for the large basin, particularly its deep ocean response (+55%). For future work, we intend to use this new framework to fit CMIP5 model temperature responses and see if it again improves upon the fits found in [Geoffroy et al., 2013].

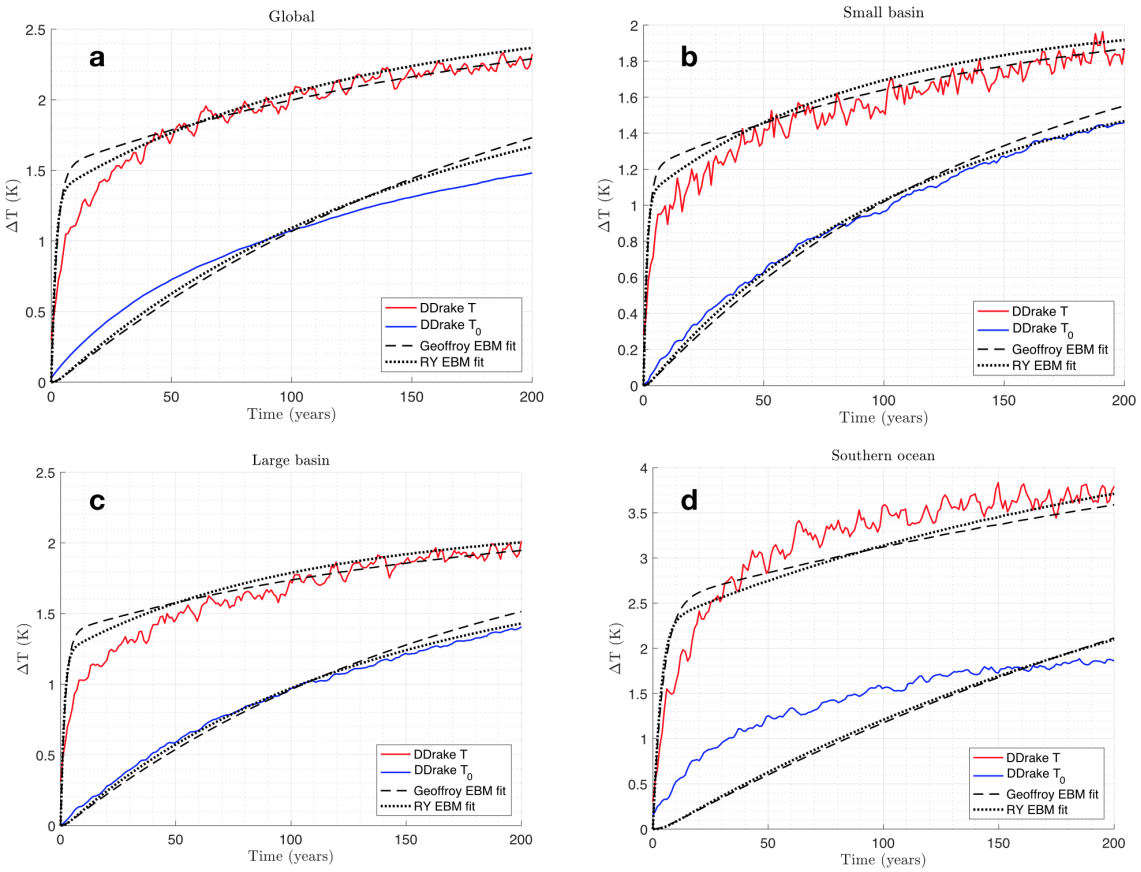


Figure 5: Time-series of annually and vertically averaged 0-50 m temperature response (red lines), 50-1050 m temperature response (blue lines); and fitted Geoffroy (black dashed) and RY (black dotted) EBM responses corresponding to the optimised heat exchange parameter values presented in table 4 for the (a) global, (b) small basin, (c) large basin, and (d) southern ocean regions of DDrake, relative to the control climate state.

## 6.1 Key points

1. Two-layer EBMs successfully reproduce the global-mean surface air temperature responses for CMIP5 models in abrupt 4x$CO_2$ experiments [Geoffroy et al., 2013]

2. The actual predicted layer temperature responses are neglected, however; particularly, the lower layer response. Plotting these for DDrake, there is very little correspondence between the layer temperature responses and Geoffroy EBM fits

3. Motivated by wind-driven circulation theory [Rhines and Young, 1982b] changing to an EBM with a quadratic heat exchange improves fits for all basins, most significantly in the large basin where wind-driven circulations dominate

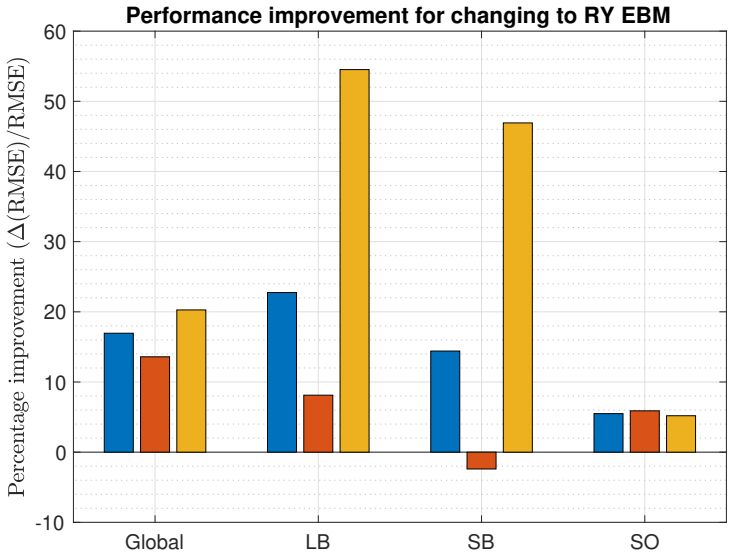


Figure 6: Percentage improvement in the RMSE of the fitted DDrake temperature responses after changing from the Geoffroy EBM to the RY EBM. Red bars are for the upper layer, yellow bars for the lower layer, and blue bars for the total. The change improves fits for all basins, but a substantial increase ($> 50\%$) is seen for the large basin lower layer temperature response.

# References

[de Boyer Montégut et al., 2004] de Boyer Montégut, C., Madec, G., Fischer, A. S., Lazar, A., and Iudicone, D. (2004). Mixed layer depth over the global ocean: An examination of profile data and a profile-based climatology. *Journal of Geophysical Research: Oceans*, 109(C12).

[Ferreira and Marshall, 2015] Ferreira, D. and Marshall, J. (2015). Freshwater transport in the coupled ocean-atmosphere system: A passive ocean. *Ocean Dynamics*, 65(7):1029–1036.

[Ferreira et al., 2015] Ferreira, D., Marshall, J., Bitz, C. M., Solomon, S., and Plumb, A. (2015). Antarctic ocean and sea ice response to ozone depletion: A two-time-scale problem. *Journal of Climate*, 28(3):1206–1226.

[Ferreira et al., 2010] Ferreira, D., Marshall, J., and Campin, J.-M. (2010). Localization of deep water formation: Role of atmospheric moisture transport and geometrical constraints on ocean circulation. *Journal of Climate*, 23(6):1456–1476.

[Frölicher et al., 2015] Frölicher, T. L., Sarmiento, J. L., Paynter, D. J., Dunne, J. P., Krasting, J. P., and Winton, M. (2015). Dominance of the southern ocean in anthropogenic carbon and heat uptake in cmip5 models. *Journal of Climate*, 28(2):862–886.

[Gent and Mcwilliams, 1990] Gent, P. R. and Mcwilliams, J. C. (1990). Isopycnal mixing in ocean circulation models. *Journal of Physical Oceanography*, 20(1):150–155.

[Geoffroy et al., 2013] Geoffroy, O., Saint-Martin, D., Olivié, D. J., Voldoire, A., Bellon, G., and Tytéca, S. (2013). Transient climate response in a two-layer energy-balance model. part i: Analytical solution and parameter calibration using cmip5 aogcm experiments. *Journal of Climate*, 26(6):1841–1857.

[Gregory and Forster, 2008] Gregory, J. and Forster, P. (2008). Transient climate response estimated from radiative forcing and observed temperature change. *Journal of Geophysical Research: Atmospheres*, 113(D23).

[Gregory et al., 2004] Gregory, J. M., Ingram, W., Palmer, M., Jones, G., Stott, P., Thorpe, R., Lowe, J., Johns, T., and Williams, K. (2004). A new method for diagnosing radiative forcing and climate sensitivity. *Geophysical research letters*, 31(3).

[Klinger et al., 1996] Klinger, B. A., Marshall, J., and Send, U. (1996). Representation of convective plumes by vertical adjustment. *Journal of Geophysical Research: Oceans*, 101(C8):18175–18182.

[Kostov et al., 2014] Kostov, Y., Armour, K. C., and Marshall, J. (2014). Impact of the atlantic meridional overturning circulation on ocean heat storage and transient climate change. *Geophysical Research Letters*, 41(6):2108–2116.

[Large et al., 1994] Large, W. G., McWilliams, J. C., and Doney, S. C. (1994). Oceanic vertical mixing: A review and a model with a nonlocal boundary layer parameterization. *Reviews of Geophysics*, 32(4):363–403.

[Marshall et al., 1997a] Marshall, J., Adcroft, A., Hill, C., Perelman, L., and Heisey, C. (1997a). A finite-volume, incompressible navier stokes model for studies of the ocean on parallel computers. *Journal of Geophysical Research: Oceans*, 102(C3):5753–5766.

[Marshall et al., 1997b] Marshall, J., Hill, C., Perelman, L., and Adcroft, A. (1997b). Hydrostatic, quasi-hydrostatic, and nonhydrostatic ocean modeling. *Journal of Geophysical Research: Oceans*, 102(C3):5733–5752.

[Molteni, 2003] Molteni, F. (2003). Atmospheric simulations using a gcm with simplified physical parametrizations. i: Model climatology and variability in multi-decadal experiments. *Climate Dynamics*, 20(2-3):175–191.

[Myhre et al., 1998] Myhre, G., Highwood, E. J., Shine, K. P., and Stordal, F. (1998). New estimates of radiative forcing due to well mixed greenhouse gases. *Geophysical research letters*, 25(14):2715–2718.

[Raper et al., 2002] Raper, S. C., Gregory, J. M., and Stouffer, R. J. (2002). The role of climate sensitivity and ocean heat uptake on aogcm transient temperature response. *Journal of Climate*, 15(1):124–130.

[Redi, 1982] Redi, M. H. (1982). Oceanic isopycnal mixing by coordinate rotation. *Journal of Physical Oceanography*, 12(10):1154–1158.

[Rhines and Young, 1982a] Rhines, P. B. and Young, W. R. (1982a). Homogenization of potential vorticity in planetary gyres. *Journal of Fluid Mechanics*, 122:347–367.

[Rhines and Young, 1982b] Rhines, P. B. and Young, W. R. (1982b). A theory of the wind-driven circulation. i. mid-ocean gyres. *J. Mar. Res*, 40(3):559–596.

[Winton, 2000] Winton, M. (2000). A reformulated three-layer sea ice model. *Journal of atmospheric and oceanic technology*, 17(4):525–531.